

Lipschitz-Margin Training: Scalable Certification of Perturbation Invariance for Deep Neural Networks

Yusuke Tsuzuku
The University of Tokyo
tsuzuku@ms.k.u-tokyo.ac.jp

Issei Sato
The University of Tokyo
RIKEN
sato@k.u-tokyo.ac.jp

Masashi Sugiyama
RIKEN
The University of Tokyo
sugi@k.u-tokyo.ac.jp

Abstract

High sensitivity of neural networks against malicious perturbations on inputs causes security concerns. We aim to ensure perturbation invariance in their predictions. However, prior work requires strong assumptions on network structures and massive computational costs, and thus their applications are limited. In this paper, based on Lipschitz constants and prediction margins, we present a widely applicable and computationally efficient method to lower-bound the size of adversarial perturbations that networks can never be deceived. Moreover, we propose an efficient training procedure to strengthen perturbation invariance. In experimental evaluations, our method showed its ability to provide a strong guarantee for even large networks.

1 Introduction

Deep neural networks are highly vulnerable against intentionally created small perturbations on inputs [37], called adversarial perturbations, which cause security concerns in applications such as self-driving cars. Image recognition systems have been intensively studied. Kurakin et al. [21] showed that adversarial perturbations indeed cause misclassifications in real-world applications. Papernot et al. [31] demonstrated how adversarial perturbations can be created without knowing the classifiers' structures.

Many heuristics have been developed to improve the robustness of neural networks against such perturbations. However, recent work repeatedly succeeded to create

adversarial perturbations for networks protected with heuristic defenses in the literature [1]. This indicates that even protected networks can be unexpectedly vulnerable. This is a crucial problem for this specific line of research because the primary concern of these studies are security threats. To tackle this crucial problem, we aim to develop defense methods with theoretical guarantees.

Our goal is to ensure the lower bounds on the size of adversarial perturbations that networks can never be deceived for each input. We refer to these lower bounds as certified invariant radii, or simply, invariant radii. To make them available in broad applications, there are two fundamental requirements to their calculation methods:

1. the minimality of assumptions on network structures,
2. the computational tractability.

However, many existing approaches require strong assumptions and massive computational costs. For example, we could not ensure perturbation invariance for some network structures such as wide residual networks [42], which have been commonly used in the evaluations of defense methods. This work tackled this problem and we provide a widely applicable, yet, highly scalable method to ensure large invariant radii.

Our basic idea is to bound the size of adversarial perturbations that networks can never be deceived. Even though the concept of using the Lipschitz constant has already appeared in Szegedy et al. [37], how much certifications they can provide has not been studied well. We show we can ensure significantly larger invariant radii compared to a recent computationally efficient counterpart [32]. However, the size of certified invariant radii can still be insufficient to be practically meaningful in some cases. We addressed this issue with a novel training procedure that further strengthen perturbation invariance. In experimental evaluations, the proposed training procedure dramatically increased invariant radii. We also observed that it could improve the robustness of networks against current attacking methods.

2 Related work

Due to severe security concerns, a number of defense methods against adversarial perturbations have been proposed. One approach is to regularize or mask gradients. Defensive distillation [30], which distills networks to themselves, is one of the most prominent methods. However, Carlini and Wagner [6] showed that adversarial perturbations can be created to deceive networks trained with defensive distillation. Input transformations and detections [40, 13] are some other defense strategies, although they can also be bypassed [5]. Adversarial training [10, 22], which injects adversarially perturbed data into training data, is a promising approach. However, there is a certain risk of overfitting to attacks [22, 38].

The existing literature indicates the difficulty in evaluating the robustness of networks. There are several studies of addressing this difficulty. One of the major

Table 1: Comparison with prior work. The columns denote (A) ability to ensure absence of adversarial perturbations, (B) ability to improve certification or empirical robustness, (C) scalability, (D) applicability to networks consisting of other activation functions than ReLU, and (E) applicability to non-smooth networks.

	(A)	(B)	(C)	(D)	(E)
Bastani+ (2015)	-	✓	-	-	✓
Katz+ (2017a;b)	✓	-	-	-	✓
Raghunathan+ (2018)	✓	✓	-	-	✓
Kolter+ (2017)	✓	✓	-	-	✓
Hein+ (2017)	✓	✓	-	✓	-
Peck+ (2017)	✓	-	✓	✓	-
Sinha+ (2018)	-	✓	✓	✓	-
Cisse+ (2017)	-	✓	✓	✓	✓
our work	✓	✓	✓	✓	✓

approaches is restricting discussion to networks using exclusively ReLU [27] for their activation functions and reduce the verification problem to some other well-studied problems. Bastani et al. [3] encoded networks to linear programs, Katz et al. [17, 16] reduced the problem to Satisfiability Modulo Theory, and Raghunathan et al. [33] encoded networks to semidefinite programs. However, these formulations demand prohibitive computational costs and their applications are limited to only small networks. As a relatively tractable method, Kolter and Wong [19] has bounded the influence of ℓ_∞ -norm bounded perturbations using convex outer-polytopes. However, it is still hard to scale this method to deep or wide networks. Another approach is assuming smoothness of networks and losses. Hein and Andriushchenko [14] focused on local Lipschitz constants of neural networks around each input. However, the guarantee is provided only for networks with one hidden layer. Peck et al. [32] bounded the size of adversarial perturbations that networks can never be deceived in a layer-wise manner. Sinha et al. [35] proposed a certifiable procedure of adversarial training. However, we cannot ensure invariant radii exactly within the framework.

Our work is an extension of Szegedy et al. [37] and its subsequent work: Parseval networks [7]. We summarized related work in Table 1.

3 Problem formulation

We define the threat model, defense goal and basic terminology.

3.1 Threat model

Let X be a sample image from data distribution D and its true label be t_X . Attackers create a new data point similar to X which deceives defenders' classifiers. As a similarity measure between data points, the ℓ_p -norms are commonly used. In this paper, we solely consider the ℓ_2 -norm as the metric.

Let c be a positive constant, and F be a classifier. We assume that the output of F is a vector $F(X)$ and the classifier predicts the label by $\operatorname{argmax}_i \{F(X)_i\}$, where $F(X)_i$ denotes the i -th element of $F(X)$. Now, we define adversarial perturbation $\epsilon_{F,X}$ as follows.

$$\epsilon_{F,X} \in \left\{ \epsilon \mid \|\epsilon\|_2 < c \wedge t_X \neq \operatorname{argmax}_i \{F(X + \epsilon)_i\} \right\}.$$

3.2 Defense goal

We define an invariant radius for the network F and the data point X as a real number c that satisfies the following condition:

$$\forall \epsilon, \left(\|\epsilon\|_2 < c \Rightarrow t_X = \operatorname{argmax}_i \{F(X + \epsilon)_i\} \right).$$

The perturbation, ϵ , with zero norm always satisfies this condition. Our goal is to ensure that neural networks have larger invariant radii for data points.

4 Overview of our work

In this section, we first describe basic concepts for calculation of invariant radii defined in Sec. 3.2. Next, we outline our training procedure to enlarge the invariant radii. Detailed proofs for inequalities and mathematical statements in Sec. 4 and Sec. 5 can be found in Appendix A of the supplementary material.

4.1 Lipschitz constant and invariant radius

We explain how to calculate the invariant radii using the Lipschitz constant. We use the same notation as that in Sec. 3. If the Lipschitz constant of neural network F is bounded by L_F , we have the following from the definition of the Lipschitz constant:

$$\|F(X) - F(X + \epsilon)\|_2 \leq L_F \|\epsilon\|_2.$$

We note that if the last layer of F is softmax, we only need to consider the subnetwork before the softmax layer. We introduce the notion of prediction margin $M_{F,X}$:

$$M_{F,X} := F(X)_{t_X} - \max_{i \neq t_X} \{F(X)_i\}.$$

This margin was previously studied in relationship with the generalization bounds [2]. Using the prediction margin, we can prove the following.

Theorem 4.1.

$$(M_{F,X} \geq \sqrt{2}L_F\|\epsilon\|_2) \Rightarrow (M_{F,X+\epsilon} \geq 0).$$

The details of the proof are in Appendix A.1 of the supplementary material. Thus, $M_{F,X}/(\sqrt{2}L_F)$ is an invariant radius for a pair F and X . This connects the Lipschitz constant, which has been discussed in Szegedy et al. [37] and Cisse et al. [7], to the absence of adversarial perturbations. Since the continuity assumption holds in many network structures, by applying this simple framework, we can address the first requirement: the minimality of assumptions. To address the second requirement: the computational tractability, we provide an efficient method to calculate the L_F in Sec. 5.

4.2 Invariant radius enlargement

To ensure large invariant radii, we propose a training procedure that enlarges the invariant radii. First of all, we provide a method to calculate L_F in a differentiable manner with respect to network parameters. This allows direct regularization of the Lipschitz constants of networks. However, based on the discussion in Sec.4.1, regularizing the Lipschitz constant can be insufficient. Instead, we aim to keep $M_{F,X}$ to be large enough compared to $\sqrt{2}L_F$. In our training procedure, a user specifies a constant c , which represents a required invariant radius for training data. During training, we add $\sqrt{2}cL_F$ to the elements of the output vector $F(X)$ before calculating the loss except for the element corresponding to class t_X . We call this training procedure *Lipschitz-Margin training* (LMT), given in Sec. 6. As long as the original training procedure performs maximization of accuracy, LMT makes invariant radii larger than c for the training data. More details on the training procedure, the interpretation of LMT, and its variants are described in Sec. 6.

5 Invariant radius calculation

In this section, we first describe a method to calculate the upper bounds of the Lipschitz constant. Then we present a variant of the invariant radius described in Sec. 4.1 and its applications.

5.1 Calculation of Lipschitz constants

We describe a method to calculate the Lipschitz constants of neural networks. We bound the Lipschitz constant of each component and recursively calculate the overall bound. This is similar to Szegedy et al. [37], but we provide more comprehensive bounds. Moreover, all our bounds can be calculated in a differentiable manner with respect to network parameters. We describe the bounds of the basic components of neural networks below.

Table 2: Notation.

W	weight matrix
$\ W\ _2$	spectral norm of W
$(ch_{\text{in}}, ch_{\text{out}})$	input and output channel size
(h_k, w_k)	kernel size
(h_s, w_s)	stride
$(h_{\text{in}}, w_{\text{in}})$	input size after padding
$\lceil r \rceil$	the smallest integer n that satisfies $n \leq r$
$\text{Diag}(r_i)$	a diagonal matrix with its i -th element is r_i

5.1.1 Composition, addition and concatenation

We describe the relationships between the Lipschitz constants and some functionals which frequently appears in deep neural networks: composition, addition and concatenation. Let f and g be functions with Lipschitz constants bounded by L_1 and L_2 , respectively. The Lipschitz constant of an output for each functional is bounded as follows:

$$\begin{aligned}
 \text{composition} & \quad f \circ g : L_1 \cdot L_2, \\
 \text{addition} & \quad f + g : L_1 + L_2, \\
 \text{concatenation} & \quad (f, g) : \sqrt{L_1^2 + L_2^2}.
 \end{aligned}$$

5.1.2 Major layers

We describe the bounds of the Lipschitz constants of major layers commonly used in image recognition tasks. Notation is summarized in Table 2. We note that we can ignore any bias parameters because they do not change the Lipschitz constants of each layer.

Fully-connected layer: The Lipschitz constant of a fully-connected layer is $\|W\|_2$. We can use a power iteration method [9] as spectral norm regularization [41] to differentially approximate $\|W\|_2$ during training. For more accurate calculation for the inference, we can use singular value decomposition.

Convolutional layer: Following Cisse et al. [7], we decompose convolution to linear operator U that repeats inputs and multiplication of matrix W . Here, W is a weight tensor of a convolution reshaped to $(ch_{\text{out}} \times ch_{\text{in}} \cdot h_k \cdot w_k)$. Carefully counting the maximum number of repetitions by U , we can bound the Lipschitz constant of U with

$$\sqrt{\left\lceil \frac{\min(h_k, h_{\text{in}} - h_k + 1)}{h_s} \right\rceil \cdot \left\lceil \frac{\min(w_k, w_{\text{in}} - w_k + 1)}{w_s} \right\rceil},$$

which is denoted by $\|U\|_2$. Then the Lipschitz constant of a convolutional layer can be bounded by $\|W\|_2 \|U\|_2$. We note that neither padding of constants before

application of U nor reshaping after multiplication W affect this bound. The obtained bound is an improvement of Cisse et al. [7].

Pooling layers: We consider an operation that splits its input x to (x_1, x_2, \dots, x_n) and apply a function f to x_i , then concatenate them: $(f(x_1), \dots, f(x_n))$. The Lipschitz constant of this operation is bounded by that of f : $\|f\|_2$. Since the pooling layers can be decomposed to an application of U and a kind of the above operation, we bound their Lipschitz constants with $\|U\|_2 \cdot \|f\|_2$. For max pooling layers, since taking max is a contraction, this is bounded by $\|U\|_2$. For average pooling layers, since the Lipschitz constant of taking the mean is bounded by $1/\sqrt{h_k w_k}$, the overall Lipschitz constant is bounded by $\|U\|_2/\sqrt{h_k w_k}$.

Normalization layers: We first consider the batch normalization layers [15]. Let γ_i and σ_i^2 be the scaling parameter and the running average of the variance of the i -th dimension, respectively. The batch normalization layer is essentially a multiplication of matrix $\text{Diag}(\gamma_i/\sqrt{\sigma_i^2 + \epsilon})$ and its Lipschitz constant is $\max_i\{|\gamma_i|/\sqrt{\sigma_i^2 + \epsilon}\}$. We note that σ_i is a constant at inference time. It is common that a batch normalization layer follows immediately after a fully-connected or a convolutional layer, In such a case, we do not have to calculate the Lipschitz constants separately; we can just replace $\|W\|_2$ in the above bounds with $\|\text{Diag}(\gamma_i/\sqrt{\sigma_i^2 + \epsilon})W\|_2$. When we apply weight normalization [34] instead of batch normalization, we can just substitute σ_i with $\|w_i\|_2$, where w_i is the i -th row of weight matrix W .

5.1.3 Activation functions

The Lipschitz constant of ReLU and tanh functions can be bounded with 1. Bounds for other major activation functions are listed in Appendix A of the supplementary material.

5.1.4 Miscellaneous processings

Preprocessing such as a mean-subtraction or a random crop has the Lipschitz constant equal to 1. If we divide each pixel by some constant s such as 255, then the Lipschitz constant of the division is $1/s$. Consider that we normalize each channel with its standard deviation. Let σ_i be the smallest standard deviation. Then, its Lipschitz constant is bounded by $1/\sigma_i$.

5.1.5 Putting them altogether

With recursive computation using the bounds described in the previous sections, we can calculate an upper bound of the Lipschitz constants of whole networks in a differential manner with respect to network parameters. As described in Sec. 4.1, the division of prediction margins by $\sqrt{2}L_F$ gives invariant radii. At inference time, calculation of the Lipschitz constant is required only once. Thus, calculation of lower bounds needs almost no computational overheads compared to the usual evaluation processes. In calculations at training time, there are some notable differences in the Lipschitz constants. For example, σ_i in a batch

normalization layer depends on the input and drop out regularization usually rescales its inputs. However, we consistently calculate the Lipschitz constants using the same bound as inference time for simplicity. Its computational cost is discussed in Sec. 6.

5.2 Variant of invariant radius

We can derive another invariant radius by decomposing classifiers to each output. Let f_i be the function defined as $f_i(X) = F(X)_i$, where $F(X)$ is defined in Sec. 3. Assuming the Lipschitz constant of $f_{t_X} - f_i$ is bounded by L_i for $i \neq t_X$, the definition of the Lipschitz constant immediately gives the following invariant radius:

$$\min_i \left\{ \frac{F(X)_{t_X} - F(X)_i}{L_i} \right\}.$$

As an example of L_i , assume that a neural classifier has a fully-connected layer as its last layer. Let L_{sub} be the Lipschitz constant of a subnetwork from its input to the input of the fully-connected layer. Let W be a weight matrix of the fully-connected layer and w_i be a row of W corresponding to a class i . In this case, we can use the following value as L_i :

$$L_{\text{sub}} \|w_{t_X} - w_i\|_2. \tag{1}$$

Even though this provides better bounds than Sec. 4.1, we have to store d^2 patterns of (1) or calculate (1) for each input, where d is a number of class labels. For applications with limited resources such as embedded systems on small devices, a bound in Sec. 4.1 can be a better option.

5.3 Comparison with Peck et al. [32]

Peck et al. [32] calculated invariant radii in layer-wise manner. Most of them can be interpreted to be bounding the Lipschitz constant of each layer. An exception is their analysis for fully-connected layers, which requires both the smoothness assumption and additional computation at inference time. Our work provides not only a different view of their work but also tighter bounds. Furthermore, we provide more comprehensive bounds for various components. A significant difference in the tightness of bounds is experimentally confirmed in Sec. 7.

5.4 Application

Since the proposed calculation method of invariant radii imposes almost no computational overhead at inference time, this property has various potential applications. First of all, we note that in real-world applications, even though true labels are not available, we can calculate the lower bounds on the size of perturbations needed to change the predictions. The primary use is balancing between the computational costs and the performance. When invariant radii are sufficiently large, we can use weak and computationally cheap detectors

of perturbations, because the detectors only need to find large perturbations. For small invariant radii, we may resort to computationally heavy options, e.g., strong detectors or denoising networks [12].

6 Defensive training

To ensure larger invariant radii, we propose a training method that encourages both small Lipschitz constants and large prediction margins. Specifically, for a given constant c , we present a method that encourages networks to have larger invariant radii than c for training data.

6.1 Lipschitz-Margin training

Based on the discussion in Sec. 4.1, to ensure that the invariant radius is larger than c , the following is a sufficient condition:

$$\forall i \neq t_X, F(X)_{t_X} > F(X)_i + \sqrt{2}cL_F.$$

Thus, we add $\sqrt{2}cL_F$ to $F(X)_i (i \neq t_X)$ at training time. We call this training procedure *Lipschitz-Margin training* (LMT). We empirically found that applying the addition only when a prediction is correct stabilizes the training. Thus, in the training, we scale the addition with

$$\alpha_{F,X} := \min_{i \neq t_X} \left\{ \max \left(0, \min \left(1, \frac{F(X)_{t_X} - F(X)_i}{\sqrt{2}cL_F} \right) \right) \right\}.$$

Even though $\alpha_{F,X}$ depends on L'_F , we do not back-propagate it. We can use the bound in Sec. 5.2 for LMT in a similar manner. The following corresponds to its sufficient condition:

$$\forall i \neq t_X, F(X)_{t_X} > F(X)_i + cL_{\text{sub}} \|w_{t_X} - w_i\|_2.$$

We refer to this as LMT++. As long as the original loss and training procedure work to maximize the training accuracy, it is clear that LMT encourages to achieve the required robustness against perturbations for training data. Its generalization to test data is experimentally evaluated in Sec. 7.

6.2 Extensions of LMT

The formulation of LMT is highly flexible, so we can consider some extended versions. First, we consider the applications that require invariant radii different in classes. For example, to distinguish humans from cats will be more important than to classify Angora cats from Persian cats. In LMT, such knowledge can be combined by specifying different hyperparameter c for each pair of classes. Second, we consider a combination of adversarial trainings. It will be more reasonable to require smaller margins for the inputs with large perturbations. In LMT, we can incorporate this intuition by changing c according to the size of perturbations or merely set c to zero for perturbed data. This ability of LMT to be easily combined with other notions is one of the advantages of LMT.

6.3 Improvements from Parseval networks

Here, we discuss the difference between our work and Cisse et al. [7]. In the formulation of Parseval networks, the goal was to limit the change in some Lipschitz continuous loss by reducing the Lipschitz constant. However, since the existence of adversarial perturbations corresponds to the 0-1 loss, which is not continuous, their discussion is not applicable. For example, if we add a scaling layer to the output of a network without changing its parameters, we can control the Lipschitz constant of the network. However, this does not change its prediction and this is irrelevant to the existence of adversarial perturbations. Therefore, considering solely the Lipschitz constant can be insufficient. In LMT, this observation is combined with training via invariant radii described in Sec. 4 and Sec. 5.

Additionally, we point out three differences. First, in Parseval networks, the upper bound of each component is restricted to be smaller than one. This makes their theoretical framework incompatible with some frequently used layers such as the batch normalization layer. Since they just ignore the effects of such layers, Parseval networks cannot control the Lipschitz constant of networks with normalization layers. On the other hand, our calculation method of invariant radii and LMT can handle such layers without problems. Second, Parseval networks force all singular values of the weight matrices to be close to one, meaning that Parseval networks prohibit weight matrices to dump unnecessary features. As Wang et al. [39] pointed out, learning unnecessary features can be a cause of adversarial perturbations, which indicates the orthonormality condition has adverse effects that encourage the existence of adversarial perturbations. Since LMT does not penalize small singular values, LMT does not suffer the problem. Third, LMT requires only differentiable bounds of the Lipschitz constants. This lets LMT be easily extended to networks with various components. On the other hand, the framework of Parseval networks requires special optimization techniques for each component.

6.4 Computational cost

A major overhead of LMT and LMT++ is calculation of the spectral norm of each weight matrix. As in spectral norm regularization, this requires only matrix-vector products. On the other hand, Parseval networks, which regularize weight matrices to be orthonormal, require the multiplications of large matrices. Even when we apply sub-sampling to reduce computation time as proposed in Cisse et al. [7], its computational complexity is larger and takes longer. If weight matrices used in networks become larger along with improvement of computation hardwares, this difference becomes more and more significant.

7 Experiments

In this section, we show the results of experimental evaluations. Since our goal is to create networks with stronger certification, we show the following three

points in the evaluations.

1. Our proposed calculation technique of invariant radii ensures the absence of adversarial perturbations for significantly larger regions compared to another computationally efficient method (Sec. 7.1).
2. LMT effectively enlarges the invariant radius (Secs. 7.1– 7.3).
3. Our invariant radius calculation and LMT are applicable to modern large and complex networks (Sec. 7.3).

We also evaluated the robustness of trained networks against current attacks (Secs. 7.2 and 7.3). For calculation of invariant radii, we used a method described in Sec. 5.2. When the test data had negative prediction margins, invariant radii were calculated as zero. We consistently calculated invariant radii in the usual scale of images, whose elements have values in range 0-255. We also used the invariant radii to calculate the upper bounds of the error ratio against the size of the perturbations. Detailed experimental setups are available in Appendix C of the supplementary material. Our codes are available at <https://github.com/ytsmiling/lmt>.

7.1 Tightness of bounds

We calculated the mean and median of normalized invariant radii on test data. For the normalization, invariant radii were divided by their input size. We used LeNet [23] on the MNIST [24] and CIFAR10 [20] datasets following Peck et al. [32]. Table 3 summarizes the results. For a reference, the median of normalized invariant radii reported in Peck et al. [32] is 6.547×10^{-8} for MNIST and 4.445×10^{-13} for CIFAR10. Invariant radii ensured by using our bounds are tens of thousand of times larger. In Table 3, we also listed invariant radii for networks trained with LMT++. Hyperparameters $c = 50$ and $c = 1$ were used for MNIST and CIFAR10, respectively. LMT++ effectively increased invariant radii and made them more than ten times larger. Since the input dimension is 784 for MNIST and 3072 for CIFAR10, a ten times larger invariant radius corresponds to a 10^{784} times larger certified region on MNIST and a 10^{3072} times larger region on CIFAR10. This supports the effectiveness of LMT++.

7.2 Effectiveness of LMT

We evaluated the effects of LMT++ on the MNIST dataset following the experimental setups of Kolter and Wong [19]. We used a network that consists of two convolutional layers and two fully connected layers. Optimizers and other hyperparameters were the same as those in Kolter and Wong [19].

General performance: Figure 1 shows the relationship between the size of perturbations and upper bounds of the error ratio on test data for different hyperparameter c of LMT++. Table 4 shows the median of invariant radii. From the derivation of LMT++, it is expected that invariant radii are larger than c .

Table 3: Statistics of invariant radii divided by input dimension. Invariant radii calculated for networks trained in a usual procedure are significantly higher than those in previous work. Moreover, LMT++ effectively enlarges them. Notation $m\cdot e\{n\}$ denotes $m \times 10^n$.

	Accuracy (Clean)	Normalized bound	
		Mean	Median
MNIST (usual)	99.3	5.918e-3	5.960e-3
MNIST (LMT++)	98.8	1.287e-1	1.316e-1
CIFAR10 (usual)	77.0	5.410e-5	4.184e-5
CIFAR10 (LMT++)	71.6	8.324e-4	6.184e-4

Table 4: Median of invariant radii on the whole test data. This corresponds to the lower bounds of the size of perturbations that can cause more than 50% error for trained networks.

c	0	1	10	100	1000
Radius	2.2	9.7	36.6	154.2	248.0

Except for the extreme case ($c = 1000$)¹, LMT++ worked as expected. This natural behavior of LMT++ is its notable property and makes it easy to tune the hyperparameter. Using LMT++ with $c = 100$, the trained network could never cause more than 6.7% and 19.2% error for any perturbations with their ℓ_2 -norm bounded by 50 and 100, respectively. Moreover, the trained network with $c = 1000$ could ensure more than 48.9% accuracy for any one-pixel attacks [36] and 44.6% accuracy for any attacks with $\|\epsilon\|_\infty \leq 10$. We emphasize that these results are fundamentally different from evaluation against some specific attacks. Even though the size of certified invariant radii is not directly comparable with that of Kolter and Wong [19] whose goal is certification against ℓ_∞ perturbations, LMT++ has a clear advantage in running time. LMT++ took less than four minutes on a single GeForce GTX 1080 Ti for training, while Kolter and Wong [19] reported that they took 10 hours on a Titan X. Moreover, our work requires almost no computational overhead to calculate invariant radii over standard evaluation processes.

To gain a better insight into the tightness of guarantee, we also calculated lower bounds of the error ratio using two adversarial attacks: DeepFool [26] and C&W attack (ℓ_2) [6]. Figure 2 shows the result against DeepFool. We can see that not only LMT++ enlarged invariant radii but also robustified networks. More precisely, in the evaluation with DeepFool, the naive network dropped

¹ For $c = 1000$, exact certification is beyond the nature of the dataset. Nevertheless, our method still provided reasonable invariant radii.

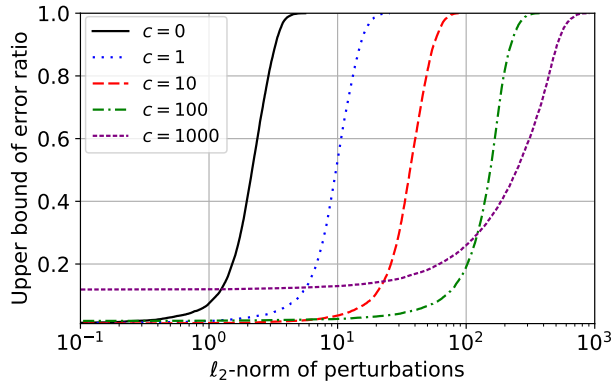


Figure 1: Relationship between the upper bounds of error ratio on test data and size of perturbations. No perturbations can cause errors beyond this bound. The term c is a hyperparameter of LMT++, which indicates the required size of invariant radii, and $c = 0$ corresponds to the usual training procedure.

its accuracy to 70.4% and 33.3% for the attacks smaller than 200 and 300 respectively. On the other hand, networks trained with LMT++ ($c = 100$) kept its accuracy at 90.1% and 79.9% for those cases. The results of the C&W attack were similar. Figures are available in Appendix D of the supplementary material. Adversarial perturbations found using DeepFool were three times larger than invariant radii on average for networks trained with LMT++ ($c = 100$). This empirically shows that the certification based on the Lipschitz constant is not too loose when we use LMT++.

Comparison with Lipschitz regularization: To evaluate the framework of LMT, we compared LMT++ with direct regularization of the Lipschitz constants. More precisely, let L be a vector with its i -th element as L_i in Sec. 5.2; we added a regularization term $\frac{\lambda}{2} \|L\|_2^2$ to the loss. We note this Lipschitz constant regularization is within the scope of our work. For a fair comparison, we searched larger hyperparameter c for LMT++ and λ for the Lipschitz constant regularization that kept error less than 2%. Figure 3 shows the difference of their effects in the upper bounds of the error ratio. Even though just regularizing the Lipschitz constant greatly improved certification, LMT++ achieved larger invariant radii. We explain the effectiveness of the Lipschitz constant regularization by the fact that the log-loss encourages larger margins even without LMT. If our objective is minimizing some Lipschitz continuous loss, it may be more reasonable to use this regularization instead of LMT. However, LMT++ showed that it could ensure larger invariant radii. This empirically supports that LMT++ tackles the targeted problem more directly.

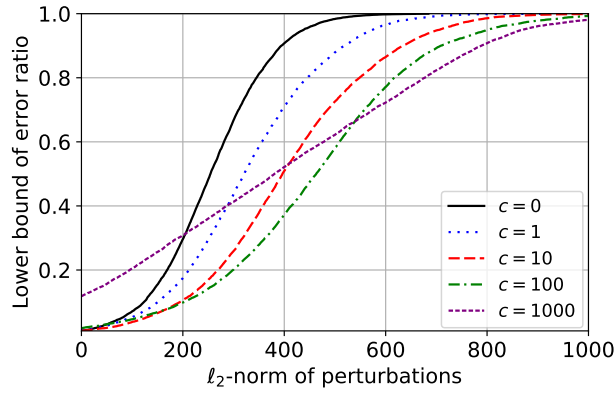


Figure 2: Lower bounds of error ratio calculated using DeepFool.

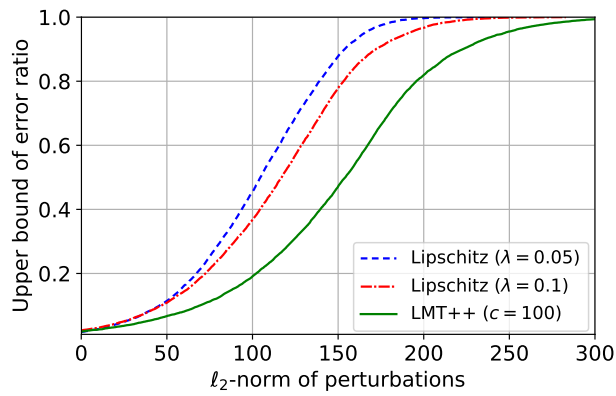


Figure 3: Comparison of direct regularizations of the Lipschitz constant and LMT++. Small upper bound indicates the method effectively increases invariant radii. Both $c = 100$ for LMT++ and $\lambda = 0.05$ for Lipschitz regularization did not cause more than 2% error on clean data, while $\lambda = 0.1$ for Lipschitz regularization did.

Table 5: Median of invariant radii on whole test data. This corresponds to the lower bounds of the size of perturbations that can cause more than 50% error for trained networks. Notation $m\text{-e}\{n\}$ denotes $m \times 10^n$. We abbreviated LMT++ as LMT.

Naive	Parseval	Spectral	LMT(0.01)	LMT(1)
6.85e-11	6.19e-7	3.76e-7	1.11e-1	3.54

7.3 Performance on large networks

We evaluated our method with a larger and more complex network to confirm broad applicability and scalability. We used 16-layered wide residual networks [42] with width factor 4 on the SVHN dataset [29] following Cisse et al. [7]. To the best of our knowledge, this is the largest network concerned with certification. We compared LMT++ with naive counterparts, spectral norm regularization [41] and Parseval networks. When we used LMT++ with $c = 1$, we decreased the hyperparameter value for of the weight decay.

Table 5 shows the median of invariant radii for each setting. LMT++ increased invariant radii by billions of times over naive counterparts. The difference with Parseval networks and the spectral norm regularization was also dramatically large. Especially, networks trained with LMT++ ($c = 1$) succeeded to ensure over 50% accuracy even for test images with 12 of their pixels are perturbed by ± 1 . LMT has two distinct features. First, it enlarges the predictions margins, which has been already discussed in Sec. 6. Second, it can deal with the normalization layers. Since the spectral norm regularization and Parseval networks do not consider the effects of the normalization layers, specifically, the batch-normalization, they failed to control the Lipschitz constants. We note that the weight decay is not an effective measure to regularize the Lipschitz constant of the batch-normalization. In the weight decay, only γ_i are regularized. On the other hand, in LMT++ and the Lipschitz constant regularization in Sec. 7.2, $\gamma_i/\sqrt{\sigma_i^2 + \epsilon}$ are regularized. This observation suggests an alternative regularization for the batch-normalization layer: applying the weight decay to $\gamma_i/\sqrt{\sigma_i^2 + \epsilon}$ instead of γ_i . Even though this regularization may improve the performance of the spectral norm regularization and Parseval networks, further investigation of this possibility is beyond the scope of this paper.

We also evaluated the robustness of trained networks against adversarial perturbations created by the current attacks. We used DeepFool for evaluation. Table 6 summarizes the results. All methods except for LMT++ with $c = 1$ kept comparable accuracy on clean data with state-of-the-art performance. We observed that Parseval networks and the spectral norm regularization make networks rather vulnerable against DeepFool. A possible explanation for this phenomenon is that well-conditioned networks make it easier for DeepFool to find small adversarial perturbations. It can be expected that since LMT++

Table 6: Accuracy of trained networks against DeepFool attack.

	Clean	Size of perturbations		
		100	200	300
Naive	98.29	74.43	35.53	11.02
Parseval	98.25	56.13	11.69	1.59
Spectral norm	98.34	64.33	18.97	3.89
LMT++ (c = 0.01)	97.97	72.90	44.57	24.73
LMT++ (c = 1)	95.25	68.10	35.82	17.83

has similar properties, it might become vulnerable against DeepFool. However, LMT++ showed improved robustness, especially against large perturbations. This indicates that the effect of LMT is significantly different from that of just controlling the distributions of singular values of the weight matrices. The difference between LMT++ with $c = 0.01$ and 0.1 was notable. This indicates that regularizing our upper bound of the Lipschitz constant is not sufficient for defending from current attacking methods and the weight decay is important to complement this. Further investigation of this possibility is left as future work.

8 Conclusion

To ensure perturbation invariance of a broad range of networks with a computationally efficient procedure, we provided a scalable certification method that uses the Lipschitz constant of networks and prediction margins. Our method can ensure the absence of adversarial perturbations for regions many orders of magnitude larger than the previous computationally efficient method. Moreover, we proposed a training procedure that makes certification significantly better. Evaluations of robustness of networks trained using our method with combinations of other heuristic defenses are left as future work.

Acknowledgement

This work was partially supported by KAKENHI 17H00757 and 17H04693.

References

- [1] N. Akhtar and A. Mian. Threat of Adversarial Attacks on Deep Learning in Computer Vision: A Survey. *CoRR*, abs/1801.00553, 2018.
- [2] P. L. Bartlett, D. J. Foster, and M. Telgarsky. Spectrally-normalized Margin Bounds for Neural Networks. In *Advances in Neural Information Processing Systems 30*, pages 6241–6250, 2017.
- [3] O. Bastani, Y. Ioannou, L. Lampropoulos, D. Vytiniotis, A. V. Nori, and A. Criminisi. Measuring Neural Net Robustness with Constraints. In *Advances in Neural Information Processing Systems 28*, pages 2613–2621, 2015.
- [4] F. Bédisle, Y. Bengio, C. Dugas, R. Garcia, and C. Nadeau. Incorporating Second-Order Functional Knowledge for Better Option Pricing. In *Advances in Neural Information Processing Systems 13*, pages 472–478, 2001.
- [5] N. Carlini and D. Wagner. Adversarial Examples Are Not Easily Detected: Bypassing Ten Detection Methods. In *Proceedings of the 10th ACM Workshop on Artificial Intelligence and Security*, pages 3–14, 2017.
- [6] N. Carlini and D. A. Wagner. Towards Evaluating the Robustness of Neural Networks. In *Proceedings of the 2017 IEEE Symposium on Security and Privacy*, pages 39–57. IEEE Computer Society, 2017.
- [7] M. Cisse, P. Bojanowski, E. Grave, Y. Dauphin, and N. Usunier. Parseval Networks: Improving Robustness to Adversarial Examples. In *Proceedings of the 34th International Conference on Machine Learning*, pages 854–863, 2017.
- [8] D. Clevert, T. Unterthiner, and S. Hochreiter. Fast and Accurate Deep Network Learning by Exponential Linear Units (ELUs). *International Conference on Learning Representations*, 2016.
- [9] G. H. G. and H. A. v. d. Vorst. Eigenvalue Computation in the 20th Century . *Journal of Computational and Applied Mathematics*, pages 35–65, 2000.
- [10] I. J. Goodfellow, J. Shlens, and C. Szegedy. Explaining and Harnessing Adversarial Examples. *International Conference on Learning Representations*, 2015.
- [11] P. Goyal, P. Dollár, R. Girshick, P. Noordhuis, L. Wesolowski, A. Kyrola, A. Tulloch, Y. Jia, and K. He. Accurate, Large Minibatch SGD: Training ImageNet in 1 Hour. *CoRR*, abs/1706.02677, 2017.

- [12] S. Gu and L. Rigazio. Towards Deep Neural Network Architectures Robust to Adversarial Examples. *International Conference on Learning Representations Workshop*, 2015.
- [13] C. Guo, M. Rana, M. Cisse, and L. v. d. Maaten. Countering Adversarial Images using Input Transformations. *International Conference on Learning Representations*, 2018.
- [14] M. Hein and M. Andriushchenko. Formal Guarantees on the Robustness of a Classifier against Adversarial Manipulation. In *Advances in Neural Information Processing Systems 30*, pages 2263–2273, 2017.
- [15] S. Ioffe and C. Szegedy. Batch Normalization: Accelerating Deep Network Training by Reducing Internal Covariate Shift. In *Proceedings of the 32nd International Conference on Machine Learning*, pages 448–456, 2015.
- [16] G. Katz, C. Barrett, D. L. Dill, K. Julian, and M. J. Kochenderfer. Towards Proving the Adversarial Robustness of Deep Neural Networks. In *Proceedings of the First Workshop on Formal Verification of Autonomous Vehicles*, pages 19–26, 2017.
- [17] G. Katz, C. W. Barrett, D. L. Dill, K. Julian, and M. J. Kochenderfer. Reluplex: An Efficient SMT Solver for Verifying Deep Neural Networks. In *Computer Aided Verification Part I*, pages 97–117, 2017.
- [18] D. P. Kingma and J. L. Ba. ADAM: A Method for Stochastic Optimization. *International Conference on Learning Representations*, 2015.
- [19] J. Z. Kolter and E. Wong. Provable Defenses against Adversarial Examples via the Convex Outer Adversarial Polytope. *Neural Information Processing Systems Workshop*, 2017.
- [20] A. Krizhevsky. Learning Multiple Layers of Features from Tiny Images. 2009.
- [21] A. Kurakin, I. Goodfellow, and S. Bengio. Adversarial Examples in the Physical World. *International Conference on Learning Representations Workshop*, 2017.
- [22] A. Kurakin, I. J. Goodfellow, and S. Bengio. Adversarial Machine Learning at Scale. *International Conference on Learning Representations*, 2017.
- [23] Y. Lecun, L. Bottou, Y. Bengio, and P. Haffner. Gradient-based Learning Applied to Document Recognition. In *Proceedings of the IEEE*, pages 2278–2324, 1998.
- [24] Y. LeCun, C. Cortes, and C. J. C. Burges. The MNIST Database of Handwritten Digits, 1998. URL <http://yann.lecun.com/exdb/mnist/>.

- [25] A. L. Maas, A. Y. Hannun, and A. Y. Ng. Rectifier Nonlinearities Improve Neural Network Acoustic Models. In *in ICML Workshop on Deep Learning for Audio, Speech and Language Processing*, 2013.
- [26] S. Moosavi-Dezfooli, A. Fawzi, and P. Frossard. DeepFool: A Simple and Accurate Method to Fool Deep Neural Networks. In *Proceedings of the IEEE Conference on Computer Vision and Pattern Recognition*, pages 2574–2582, 2016.
- [27] V. Nair and G. E. Hinton. Rectified Linear Units Improve Restricted Boltzmann Machines. In *Proceedings of the 27th International Conference on Machine Learning (ICML-10), June 21-24, 2010, Haifa, Israel*, 2010.
- [28] Y. Nesterov. A Method for Unconstrained Convex Minimization Problem with the Rate of Convergence $o(1/k^2)$. *Soviet Mathematics Doklady*, pages 372–376, 1983.
- [29] Y. Netzer, T. Wang, A. Coates, A. Bissacco, B. Wu, and A. Y. Ng. Reading Digits in Natural Images with Unsupervised Feature Learning. *Neural Information Processing Systems Workshop*, 2011.
- [30] N. Papernot, P. D. McDaniel, X. Wu, S. Jha, and A. Swami. Distillation as a Defense to Adversarial Perturbations Against Deep Neural Networks. In *Proceedings of the IEEE Symposium on Security and Privacy*, pages 582–597, 2016.
- [31] N. Papernot, P. D. McDaniel, I. J. Goodfellow, S. Jha, Z. B. Celik, and A. Swami. Practical Black-Box Attacks against Machine Learning. In *Proceedings of the 2017 ACM on Asia Conference on Computer and Communications Security, AsiaCCS 2017, Abu Dhabi, United Arab Emirates, April 2-6, 2017*, pages 506–519, 2017.
- [32] J. Peck, J. Roels, B. Goossens, and Y. Saeys. Lower Bounds on the Robustness to Adversarial Perturbations. In *Advances in Neural Information Processing Systems 30*, pages 804–813, 2017.
- [33] A. Raghunathan, J. Steinhardt, and P. Liang. Certified Defenses against Adversarial Examples. *International Conference on Learning Representations*, 2018.
- [34] T. Salimans and D. P. Kingma. Weight Normalization: A Simple Reparameterization to Accelerate Training of Deep Neural Networks. In *Advances in Neural Information Processing Systems 29*, pages 901–909, 2016.
- [35] A. Sinha, H. Namkoong, and J. Duchi. Certifiable Distributional Robustness with Principled Adversarial Training. *International Conference on Learning Representations*, 2018.
- [36] J. Su, D. V. Vargas, and S. Kouichi. One pixel attack for fooling deep neural networks. *CoRR*, 2017.

- [37] C. Szegedy, W. Zaremba, I. Sutskever, J. Bruna, D. Erhan, I. J. Goodfellow, and R. Fergus. Intriguing Properties of Neural Networks. *International Conference on Learning Representations*, 2014.
- [38] F. Tramèr, A. Kurakin, N. Papernot, D. Boneh, and P. D. McDaniel. Ensemble Adversarial Training: Attacks and Defenses. *International Conference on Learning Representations*, 2018.
- [39] B. Wang, J. Gao, and Y. Qi. A Theoretical Framework for Robustness of (Deep) Classifiers against Adversarial Examples. *International Conference on Learning Representations Workshop*, 2017.
- [40] W. Xu, D. Evans, and Y. Qi. Feature Squeezing: Detecting Adversarial Examples in Deep Neural Networks. *Network and Distributed Systems Security Symposium*, 2018.
- [41] Y. Yoshida and T. Miyato. Spectral Norm Regularization for Improving the Generalizability of Deep Learning. *CoRR*, abs/1705.10941, 2017.
- [42] S. Zagoruyko and N. Komodakis. Wide Residual Networks. In *Proceedings of the British Machine Vision Conference*, pages 87.1–87.12, 2016.

A Proofs of inequalities

In this section, we provide proofs used in Sec. 4 and Sec. 5.

A.1 Relationship between Lipschitz constant and prediction margin

Let us consider a classifier with its Lipschitz constant being bounded with a constant L . Let $F(X)$ be an output vector of the classifier for a data point X .

Proof of Theorem 4.1:

The statement to prove is the following:

$$F(X)_{t_X} - \max_{i \neq t_X} F(X)_i \geq \sqrt{2}L\|\epsilon\|_2 \Rightarrow F(X + \epsilon)_{t_X} - \max_{i \neq t_X} F(X + \epsilon)_i \geq 0. \quad (2)$$

If we prove the following, it suffices:

$$F(X + \epsilon)_{t_X} - \max_{i \neq t_X} F(X + \epsilon)_i \geq F(X)_{t_X} - \max_{i \neq t_X} F(X)_i - \sqrt{2}L\|\epsilon\|_2. \quad (3)$$

Before proving inequality (3), we have the following lemma.

Lemma A.1. *For real vectors x and y , the following inequality holds:*

$$\left| \max_{i \neq t_X} x_i - \max_{i \neq t_X} y_i \right| \leq \max_{i \neq t_X} |x_i - y_i|. \quad (4)$$

Let j be $\operatorname{argmax}_{i \neq t_X} x_i$ and k be $\operatorname{argmax}_{i \neq t_X} y_i$. Note that $j \neq t_X$ and $k \neq t_X$.

$$\begin{aligned} -\max_{i \neq t_X} |x_i - y_i| &\leq -|x_k - y_k| \\ &\leq x_k - y_k \\ &= x_k - \max_{i \neq t_X} y_i \\ &\leq \max_{i \neq t_X} x_i - \max_{i \neq t_X} y_i \end{aligned}$$

and

$$\begin{aligned} \max_{i \neq t_X} x_i - \max_{i \neq t_X} y_i &= x_j - \max_{i \neq t_X} y_i \\ &\leq x_j - y_j \\ &\leq |x_j - y_j| \\ &\leq \max_{i \neq t_X} |x_i - y_i|. \end{aligned}$$

Thus, inequality (4) holds. \square

Now, we can prove the inequality (3).

$$\begin{aligned}
& F(X + \epsilon)_{t_X} - \max_{i \neq t_X} F(X + \epsilon)_i \\
&= F(X)_{t_X} - \max_{i \neq t_X} F(X)_i + (F(X + \epsilon)_{t_X} - F(X)_{t_X}) - \left(\max_{i \neq t_X} F(X + \epsilon)_i - \max_{i \neq t_X} F(X)_i \right) \\
&\geq F(X)_{t_X} - \max_{i \neq t_X} F(X)_i - |F(X + \epsilon)_{t_X} - F(X)_{t_X}| - \left| \max_{i \neq t_X} F(X + \epsilon)_i - \max_{i \neq t_X} F(X)_i \right| \\
&\geq F(X)_{t_X} - \max_{i \neq t_X} F(X)_i - |F(X + \epsilon)_{t_X} - F(X)_{t_X}| - \max_{i \neq t_X} |F(X + \epsilon)_i - F(X)_i| \\
&\geq F(X)_{t_X} - \max_{i \neq t_X} F(X)_i - \max \left\{ |a_1| + |a_2| \left| \sqrt{a_1^2 + a_2^2} \leq L \|\epsilon\|_2 \right. \right\} \\
&= F(X)_{t_X} - \max_{i \neq t_X} F(X)_i - \sqrt{2}L \|\epsilon\|_2.
\end{aligned}$$

Thus, the statement (2) holds. \square

A.2 Lipschitz constant of basic components

We prove bounds described in Sec. 5.1.1. Let f and g be functions with their Lipschitz constants bounded with L_1 and L_2 , respectively.

A.2.1 Composition of functions

$$\begin{aligned}
& \frac{\|f(g(X_1)) - f(g(X_2))\|_2}{\|X_1 - X_0\|_2} \\
&= \frac{\|f(g(X_1)) - f(g(X_2))\|_2}{\|g(X_1) - g(X_2)\|_2} \cdot \frac{\|g(X_1) - g(X_2)\|_2}{\|X_1 - X_0\|_2} \\
&\leq L_1 \cdot \frac{\|g(X_1) - g(X_2)\|_2}{\|X_1 - X_0\|_2} \\
&\leq L_1 \cdot L_2.
\end{aligned}$$

A.2.2 Addition of functions

Using triangle inequality,

$$\begin{aligned}
& \frac{\|(f + g)(X_1) - (f + g)(X_2)\|_2}{\|X_1 - X_0\|_2} \\
&\leq \frac{\|f(X_1) - f(X_2)\|_2 + \|g(X_1) - g(X_2)\|_2}{\|X_1 - X_0\|_2} \\
&\leq L_1 + L_2.
\end{aligned}$$

A.2.3 Concatenation of functions

$$\begin{aligned}
& \frac{\|(f(X_1), g(X_1)) - (f(X_0), g(X_0))\|_2}{\|X_1 - X_0\|_2} \\
&= \sqrt{\frac{\|(f(X_1), g(X_1)) - (f(X_0), g(X_0))\|_2^2}{\|X_1 - X_0\|_2^2}} \\
&= \sqrt{\frac{\|f(X_1) - f(X_0)\|_2^2 + \|g(X_1) - g(X_0)\|_2^2}{\|X_1 - X_0\|_2^2}} \\
&\leq \sqrt{L_1^2 + L_2^2}.
\end{aligned}$$

A.3 Lipschitz constant of layers

We first prove the bound for convolutional layer following Cisse et al. [7]. Next, we extend the work and prove more tight and various bounds. We use the same notation as in Sec. 5.1.2.

A.3.1 Convolutional layers

We assume all paddings are constant paddings, like zero-paddings. We note that constant padding can be a concatenation of a constant function with the Lipschitz constant as zero, and from Appendix A.2, it does not affect the upper bounds of the Lipschitz constants.

We first derive the following bound of Lipschitz constant for a convolutional layer,

$$L \leq \sqrt{h_k \cdot w_k} \cdot \|W\|_2,$$

which was derived by Cisse et al. [7].

Let ch_{in} and ch_{out} be the channel sizes of the input and output, respectively. Let us decompose the operation of convolution into a composition of a linear operator U and a matrix multiplication W . Here, matrix W is a weight tensor of convolution, reshaped to $(ch_{out} \times ch_{in} \cdot h_k \cdot w_k)$. Operation U repeats each element of the inputs for $h_k \cdot w_k$ times at most. Since a repetition is a concatenation of the same function, the Lipschitz constant of U is bounded by $\sqrt{h_k \cdot w_k}$. Thus, the Lipschitz constant of $W \circ U$ can be bounded by $\sqrt{h_k \cdot w_k} \|W\|_2$. the reshape may follow after the multiplication of W ; however, this does not increase the Lipschitz constant. \square

Now, we extend the bound by considering the input size and stride. Firstly, we consider the input size after padding. If both the input and kernel size are 8×8 , the repetition by U is obviously bounded by 1. Similarly, the repeat by U can be bounded by the following:

$$\min(h_k, h_{in} - h_k + 1) \cdot \min(w_k, w_{in} - w_k + 1).$$

We can further bound the time of repeat by considering the stride as follows:

$$\left\lceil \frac{\min(h_k, h_{in} - h_k + 1)}{h_s} \right\rceil \cdot \left\lceil \frac{\min(w_k, w_{in} - w_k + 1)}{w_s} \right\rceil.$$

Thus, we can improve the Lipschitz constant of U by the following:

$$\sqrt{\left\lceil \frac{\min(h_k, h_{in} - h_k + 1)}{h_s} \right\rceil} \cdot \left\lceil \frac{\min(w_k, w_{in} - w_k + 1)}{w_s} \right\rceil.$$

This improvement is especially important in layers with the small width and height of inputs.

A.3.2 Pooling layers

We will now describe the bounds for pooling layers. We use the same notation as in the previous section. First, we prove the following lemma:

Lemma A.2. *Let vector X be a concatenation of vectors X_i ($0 \leq i \leq n$) and let f be a function such that $f(x)$ is a concatenations of vectors $f_i(X_i)$, where each f_i is a function with its Lipschitz constant bounded by L_0 (≥ 0). Then, the Lipschitz constant of f can be bounded by L_0 .*

$$\begin{aligned} \frac{\|f(X) - f(Y)\|_2^2}{\|X - Y\|_2^2} &= \frac{\sum_i \|f_i(X_i) - f_i(Y_i)\|_2^2}{\|X - Y\|_2^2} \\ &\leq \frac{\sum_i L_0^2 \|X_i - Y_i\|_2^2}{\|X - Y\|_2^2} \\ &= L_0^2 \end{aligned}$$

□

In pooling layers, each channel of the input corresponds to X_i , and f can be written in the form of the lemma. Next, we bound each f_i for average and pooling layers. We note that every f_i is the same in pooling layers.

In max pooling, f_i is a composition of operator U and max function in Sec. A.3.1. Taking max is obviously a contraction and the Lipschitz constant of max-pooling layer is bounded by $\|U\|_2$.

In average pooling, f_i is a composition of operator U and the average function. The input size of the average function is $h_k \cdot w_k$. Before bounding the Lipschitz constant, we note the following inequality for vector X :

$$\left(\sum_{i=1}^n X_i \right)^2 \leq n \sum_{i=1}^n X_i^2.$$

This can be proved using

$$\frac{1}{n} \sum_{i=1}^n X_i^2 - \left(\frac{1}{n} \sum_{i=1}^n X_i \right)^2 = \frac{1}{n} \sum_{i=1}^n \left(X_i - \frac{1}{n} \sum_{i=1}^n X_i \right)^2 \geq 0.$$

Now, we bound the Lipschitz constant of the average function $\text{Avg}(\cdot)$.

$$\begin{aligned} \frac{\|\text{Avg}(X) - \text{Avg}(Y)\|_2}{\|X - Y\|_2} &= \frac{|\text{Avg}(X - Y)|}{\|X - Y\|_2} \\ &= \frac{|\sum_{i=1}^{h_k \cdot w_k} (X_i - Y_i)|}{\|X - Y\|_2} / (h_k \cdot w_k) \\ &\leq \frac{1}{\sqrt{h_k \cdot w_k}}. \end{aligned}$$

Thus, the overall Lipschitz constant is bounded by $\|U\|_2 / \sqrt{h_k \cdot w_k}$. Note that these bounds are clearly better than those provided by Peck et al. [32], where bounds are made by the output size of the layers.

A.3.3 Normalization layers

We first consider a batch normalization layer. Batch normalization applies the following function element,

$$x_i \leftarrow \gamma_i \frac{x_i - \mu_i}{\sqrt{\sigma_i^2 + \epsilon}} + \beta_i, \quad (5)$$

where γ_i and β_i are the learned parameters and μ_i, σ_i are the running mean and deviation, respectively. Small constant ϵ is generally added for numerical stability. γ_i, β_i, μ_i , and σ_i are tied in each channel in convolutional layers. We can rewrite an update of (5) as follows:

$$x_i \leftarrow \frac{\gamma_i}{\sqrt{\sigma_i^2 + \epsilon}} x_i + \left(-\gamma_i \frac{\mu_i}{\sqrt{\sigma_i^2 + \epsilon}} + \beta_i\right).$$

Since the second term is constant in terms of input, it is independent of the Lipschitz constant. Thus, we consider the following update:

$$x_i \leftarrow \frac{\gamma_i}{\sqrt{\sigma_i^2 + \epsilon}} x_i.$$

The Lipschitz constant can be bounded by $\max_i \{|\gamma_i| / \sqrt{\sigma_i^2 + \epsilon}\}$.

In the cases when the batch normalization layer succeeds immediately a fully-connected or a convolutional layer, which frequently happen in modern networks, we can obtain a better bound. The overall operation can be written as an application of two matrix multiplications:

$$\text{Diag} \left(\frac{|\gamma_i|}{\sqrt{\sigma_i^2 + \epsilon}} \right) \circ W.$$

Thus, replacing the spectral norm of W by that of $\text{Diag} \left(|\gamma_i| / \sqrt{\sigma_i^2 + \epsilon} \right) W$ in bounds of fully-connected and convolutional layers provides bounds of the composition of two layers.

Table 7: Lipschitz constants of major activation functions.

Activation	Lipschitz constant
ReLU	1
Leaky ReLU [25]	$\max(1, \alpha)$
sigmoid	1/4
tanh	1
soft plus [4]	1
ELU [8]	$1 \max(1, \alpha)$

A.4 Activation functions

Table 7 lists up the Lipschitz constants of activation functions and other nonlinear functions commonly used in deep neural networks.

B Calculation of spectral norm

In this section, we describe our implementation for calculation of the spectral norms.

B.1 Basics of spectral norm regularization

We will explain here how to calculate the spectral norms of the matrices, following Yoshida and Miyato [41]. Using the power iteration method [9], we can approximate the spectral norm of the matrices. Let A be a matrix with its shape $N \times M$ and u, v be the vectors with sizes N and M , respectively. We consider the following procedure:

$$\begin{aligned} u &\leftarrow Av / \|Av\|_2, \\ v &\leftarrow A^T u / \|A^T u\|_2. \end{aligned}$$

Starting with randomly initialized v , u and v converge to the left and right singular vectors of the largest singular value, respectively. Thus, after convergence, we can gain the largest singular value with

$$\|A\|_2 = u^T Av.$$

Since the weight matrices do not change significantly between consecutive training iterations, we can use v as the previous iteration for the initial value, as just one iteration is enough to get good approximations.

B.2 Implementation

To regularize the spectral norms more correctly, we used different u and v between the forward and backward paths like it was done by Yoshida and Miyato

Table 8: Network structure used for experiment 7.1. For convolutional layers, output size denotes channel size of output.

	output size	kernel	padding	stride
convolution	20	(5,5)	(0,0)	(1,1)
max-pooling	-	(2,2)	(0,0)	(2,2)
ReLU	-	-	-	-
convolution	50	(5,5)	(0,0)	(1,1)
max-pooling	-	(2,2)	(0,0)	(2,2)
ReLU	-	-	-	-
fully-connected	500	-	-	-
ReLU	-	-	-	-
fully-connected	10	-	-	-

[41]. We describe the details based on our implementation. In forward path, the spectral norm s was calculated as follows:

$$\begin{aligned} v &\leftarrow A^T u_1 / \|A^T u_1\|_2, \\ u_2 &\leftarrow Av, \\ s &\leftarrow \|u_2\|_2. \end{aligned}$$

In backward path, assuming both u_2 and v were normalized, gradients were calculated as follows:

$$\frac{\partial s}{\partial A} = u_2 v^T.$$

We also used this technique for the joint calculation of the Lipschitz constant of the convolutional layer and the batch normalization layer.

C Experimental setups

In this section, we describe the details of our experimental settings.

C.1 Experiment 7.1

LeNet [23] based architecture was used consisting of two convolutional layers and two fully-connected layers. Table C.1 shows the details of its structure.

For MNIST dataset, all inputs were divided by 255 before the first layer of the network. The Lipschitz constant of this operation is bounded by $1/255$. For CIFAR10 dataset, all channels of the inputs were subtracted by their means of the training data. Then, they were divided by their standard deviation. The Lipschitz constant of this operation is bounded by $\min_{\text{channel}}\{1/\sigma_{\text{channel}}\}$.

Table 9: Network structure used for experiment 7.2. For convolutional layers, output size denotes channel size of output.

	output size	kernel	padding	stride
convolution	16	(4,4)	(1,1)	(2,2)
ReLU	-	-	-	-
convolution	32	(4,4)	(1,1)	(2,2)
ReLU	-	-	-	-
fully-connected	100	-	-	-
ReLU	-	-	-	-
fully-connected	10	-	-	-

Training images were padded by zero with 4 pixels on each side and randomly cropped to original size. They were horizontally flipped with probability 0.5. Models were trained with Momentum SGD for 20 epochs with a batch size of 128. The initial learning rate was set to 0.1 and it was halved at every 5 epochs.

C.2 Experiment 7.2

A network consisting of two convolutional and two fully-connected layers was used. Table C.2 shows the details of its structure.

All inputs were divided by 255 before the first layer of the network. The Lipschitz constant of this operation is bounded by $1/255$.

Models were trained using Adam optimizer [18] for 20 epochs with a batch size of 50. The learning rate of Adam was set to 0.001.

C.3 Experiment 7.3

Wide residual network [42] with 16 layers and a width factor $k = 4$ was used. We sampled 10000 images from an extra data available for SVHN dataset as validation data and combined the rest with the official training data, following Cisse et al. [7]. All inputs were divided by 255 before the first layer of the network. The Lipschitz constant of this operation is bounded by $1/255$.

Models were trained with Nesterov Momentum [28] for 160 epochs with a batch size of 128. The initial learning rate was set to 0.01 and it was multiplied by 0.1 at epochs 80 and 120. For naive models, the weight decay with $\lambda = 0.0005$ and the dropout with a dropout ratio of 0.4 were used. For Parseval networks, the weight decay was removed except for the last fully-connected layer and Parseval regularization with $\beta = 0.0001$ was added, following Cisse et al. [7]. For a network with the spectral norm regularization, the weight decay was removed and the spectral norm regularization with $\lambda = 0.01$ was used following Yoshida and Miyato [41]. We note that both Cisse et al. [7] and Yoshida and Miyato [41] used batch-normalization for their experimental evaluations and thus, we

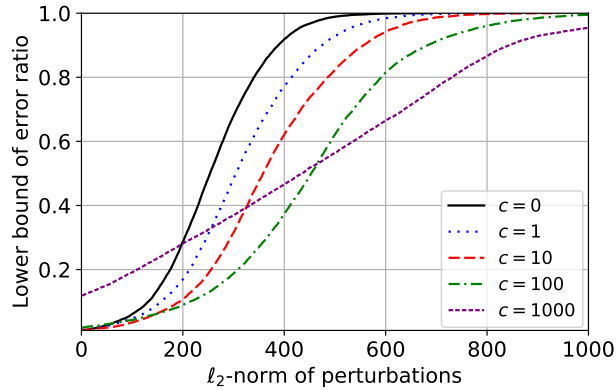


Figure 4: Lower bounds of error ratio calculated using C&W attack.

left it for them. For LMT++ with $c = 1$, we decreased the hyperparameter λ of the weight decay to 0.0001. We set an initial value of c to 0.001 and linearly increased it to 1 in first 5 epochs as learning rate scheduling used in Goyal et al. [11]. For LMT++ with $c = 0.01$, we used the same configuration with naive counterparts. In residual blocks, the Lipschits constant for the convolutional layer and the batch normalization layer was jointly calculated as described in Sec. 5.1.2.

D Additional experimental results

In this section, we provide additional experimental results.

D.1 Evalutaion with C&W attack in Experiment 7.2

Figure 4 is a results of evaluation using C&W attack in experiment 7.2. The results were similar with evaluation using DeepFool.